Enhanced stimulated Raman scattering during intense laser propagation

J. Ryan Peterson,[1,2,*] **Theodore G. Jones,**[3] **Bahman Hafizi** [3]
Luke A. Johnson [3] **Daniel F. Gordon** [3] **Yu-Hsin Chen** [3]
Antonio Ting [4]

[1] *Physics Department, Stanford University, 450 Serra Mall, Stanford, CA 94305*
[2] *SLAC National Accelerator Laboratory, 2575 Sand Hill Rd, Menlo Park, CA 94025*
[3] *Directed Energy Physics Branch, Plasma Physics Division, Naval Research Laboratory, 4555 Overlook Ave SW, Washington, DC 20375*
[4] *Commonwealth Technology Innovation LLC, Alexandria, VA 22315*
[*] *jrpete@stanford.edu*

Abstract: Stimulated Raman scattering is ubiquitous in many high-intensity laser environments. Parameteric four-wave mixing between the pump and Raman sidebands can affect the Raman gain, but stringent phase matching requirements and strongly nonlinear dynamics obscure clear understanding of its effects at high laser powers. Here we investigate four-wave mixing in the presence of strong self-focusing and ionization at laser powers above the Kerr critical power. Theoretical analysis shows that the plasma generated at focus naturally leads to proper phase matching for enhanced Raman gain almost without regard to the initial phase mismatch. Multidimensional nonlinear optical simulations with multiphoton and collisional ionization confirm the enhancement and suggest that it may lead to significantly higher Raman losses in some nonlinear laser propagation environments.

1. Introduction

A variety of nonlinear effects arise during intense laser propagation in dielectrics. Among these is stimulated Raman scattering (SRS), which transfers laser energy to both the medium and optical sidebands. Significant efforts have been expended to understand and measure SRS, including in water [1–3]; although SRS can be sometimes beneficial [4] and other times detrimental [5], both cases require a good understanding of the factors affecting SRS gain.

Stimulated Raman scattering is long known to be affected by parametric four-wave mixing (FWM) between the laser and the two Raman sidebands [6]. The coupled system can experience either suppressed or enhanced Raman gain, both of which have been investigated theoretically and experimentally in fibers with laser power of order 100 W [7–11]. The coupled gain depends sensitively on the phase mismatch, which was optimized in experiments by tuning the laser wavelength, power, pump-probe propagation angle, and/or using purpose-built fibers. These results may be important for fiber applications, where both the laser and material parameters can be carefully controlled. However, in non-phase-matched systems such as in laser nanosurgery [12], water-based frequency conversion [4] and underwater acoustic generation [5, 13, 14], the impact of FWM is less clear.

At high laser powers exceeding the Kerr critical power (of order 1 MW in condensed media), the influence of FWM is obscured by several highly nonlinear effects. The laser will self-focus until it ionizes the medium and plasma defocusing counteracts self-focusing. The presence of the plasma, as well as the range of propagation angles inherent to a focusing beam, greatly complicate the SRS gain. We can progress theoretically, however, by limiting our analysis to the weakly-ionized ($< 1\%$) regime, where SRS is still determined largely by the medium response. Further, above the critical power, the plasma and Kerr response at focus are strongly connected which allows us to understand the phase matching. Finally, we turn to the SNOPROP simulation code to solve the full three-envelope nonlinear propagation equations with SRS, FWM, the optical Kerr effect, and multiphoton and collisional ionization in 2D cylindrical geometry [15, 16].

We find that the self-generated plasma can strongly enhance the SRS gain. Analytic theory demonstrates that at high intensities, the self-generated plasma dispersion provides nearly optimal phase matching for maximum Raman gain, almost without regard to the initial phase mismatch. Multidimensional numerical simulations of a few-MW picosecond laser focusing in water confirm the SRS gain enhancement and agree well with analytic theory. Laser energy losses to the Stokes Raman band can increase by a factor of several due to the enhanced gain.

2. Theoretical analysis

We consider an envelope propagation model including beams at the Raman Stokes, laser, and Raman anti-Stokes frequencies $\omega_S = \omega_L - \omega_v$, ω_L, and $\omega_A = \omega_L + \omega_v$ respectively, where ω_v is the vibrational Raman frequency. The total electric field has the form

$$\mathbf{E}(\vec{r}, t) = \mathbf{e}_x \sum_{n=S,L,A} \left(A_n e^{-i(\beta(\omega_n)z - \omega_n t)} + \text{c.c.} \right), \tag{1}$$

where $\mathbf{e}_x$ is the unit vector in the x-direction, A_n the envelope field, and $\beta(\omega_n) = k_n$ the wavenumber, and a subscript $n \in \{S, L, A\}$ corresponds to the Stokes, laser, or anti-Stokes beam respectively. The three beams interact in the presence of a third-order resonant (Raman) susceptibility χ_{RS} and nonresonant (Kerr) susceptibility χ_{NR} as well as a self-generated plasma. We restrict our analysis to the the propagation of an above-critical power laser pulse propagating in a weakly-ionized dielectric. We also include several numerical examples in the case of a laser with wavelength $\lambda_L = 355$ nm propagating in water, whose Raman frequency is $\omega_v = 6.4 \times 10^{14}$ s^{-1}, resonant susceptibility $\chi_{RS} = -1.1i \times 10^{-18}$ cm^2/V^2, and nonresonant susceptibility $\chi_{NR} = 3.3 \times 10^{-18}$ cm^2/V^2 [3].

We begin in the strong, static pump approximation by assuming $|A_L| \gg |A_S|$, $|A_L| \gg |A_A|$, and $|A_L|$ is constant, and we neglect transverse effects, ionization losses, and self-phase modulation. In this case the propagation equations for the Stokes and anti-Stokes waves reduce to the coupled equations

$$\frac{\partial A_S}{\partial z} = -\alpha_1 A_S + \kappa_1 A_A^* e^{i\Delta k z} \tag{2a}$$

$$\frac{\partial A_A}{\partial z} = -\alpha_2 A_A + \kappa_2 A_S^* e^{i\Delta k z}, \tag{2b}$$

where α_1, α_2, κ_1, and κ_2 are constant coefficients which may include the effects of SRS, FWM, cross-phase modulation (the optical Kerr effect) and plasma refraction, and $\Delta k = 2k_L - k_S - k_A$ is the wavevector mismatch.

The general solution to a system of the form in Eqs. 2a and 2b was first given by Bloembergen [6]. The dominant mode A_+, a linear combination of A_S and A_A, will evolve according to $A_+ \propto e^{gz}$ where

$$g = -\frac{1}{2}(\alpha_1 + \alpha_2^*) + \frac{1}{2} \left[(\alpha_1 - \alpha_2^* + i\Delta k)^2 + 4\kappa_1 \kappa_2^* \right]^{1/2}, \tag{3}$$

meaning that the real part, $\text{Re}[g]$, is the gain coefficient.

2.1. Stimulated Raman Scattering

Equation 3 has been studied both analytically and experimentally in various limits [6, 8, 9, 17]. To understand the combined effects of SRS, FWM, the optical Kerr effect, and ionization, it is useful to start by reviewing each of the effects in turn. Beginning with only SRS (and neglecting FWM, Kerr, and plasma) requires $\alpha_1 = -\alpha_R$, $\alpha_2 = h\alpha_R$, and $\kappa_1 = \kappa_2 = 0$, where

$\alpha_R = 3i\omega_S\chi_{RS}|A_L|^2/(cn_S)$ is the Raman gain coefficient in the absence of four-wave mixing, $h = \omega_A n_S/(\omega_S n_A)$ a constant, c the speed of light, and $n_n = ck_n/\omega_n$ the linear index of refraction at frequency ω_n. Note that because χ_{RS} is negative imaginary, the gain coefficient α_R is positive real. In this simplest case the Stokes sideband gains energy from the laser while the anti-Stokes sideband loses energy to the laser.

2.2. Four-Wave Mixing

The dynamics become more complicated when the anti-Stokes and Stokes sidebands are allowed to exchange energy with each other due to four-wave mixing. We consider both SRS and FWM by setting $\kappa_1 = \alpha_R$ and $\kappa_2 = -h\alpha_R$ with $\alpha_1 = -\alpha_R$ and $\alpha_2 = h\alpha_R$ as before. Here both the Stokes and anti-Stokes waves will experience gain with a coefficient depending on the phase mismatch Δk. Figure 1(a) illustrates the gain spectrum in water at 355 nm ($\Delta k = -550$ cm^{-1}) for several laser intensities. In the case of a large phase mismatch, $|\Delta k| \gg \alpha_R$, the coupled gain Re[g] asymptotes to the uncoupled Raman gain coefficient α_R; although both waves experience gain, the dominant mode A_+ will be composed almost entirely of Stokes light with very little anti-Stokes light [17]. In the phase-matched case where $|\Delta k| = 0$, the waves can transfer energy extremely efficiently, as demonstrated experimentally in silica fibers [18]. However, in this case the coupled gain drops to 0; since the Stokes and anti-Stokes waves are perfectly coupled, any laser energy given to the Stokes wave is easily transferred to the anti-Stokes wave and then back to the laser. This gain suppression when $\delta k \ll \alpha_R$ near perfect phase matching has also been demonstrated experimentally [8].

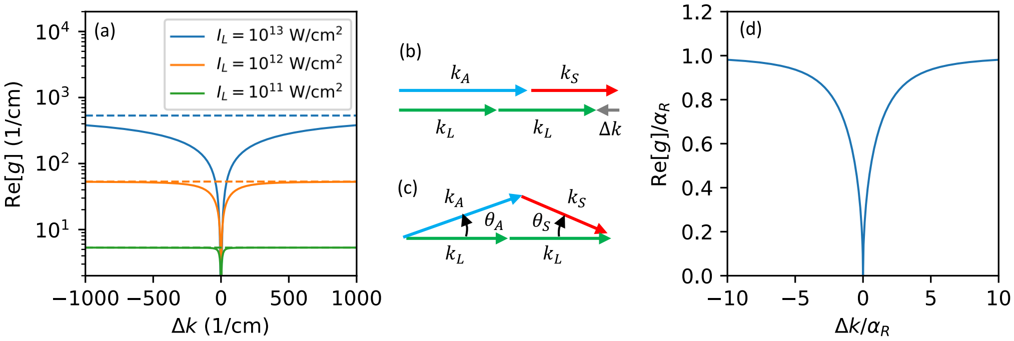

Fig. 1. Coupled gain spectrum including four-wave mixing. (a) Coupled gain (solid lines) and decoupled gain (dashed lines) in water for a 355 nm laser with three different intensities. (b) Phase mismatch Δk depicted for copropagating beams in a material with normal dispersion. (c) The phase mismatch Δk may be eliminated if the Stokes and anti-Stokes beams propagate off-axis from the laser. (d) The approximate coupled gain spectrum normalized to the decoupled gain α_R is valid at any intensity.

The magnitude of the phase mismatch depends on the material dispersion as well as the relative orientation of the laser, Stokes, and anti-Stokes beams. In the copropagating case shown in Fig. 1(b), the phase mismatch is always negative (positive) in media with normal (anomalous) dispersion near the laser wavelength, and vanishes only near the zero-dispersion wavelength. Experiments with two input beams can phase match by orienting the laser and Stokes beams at a small angle θ_S with respect to each other, which will produce an anti-Stokes beam oriented slightly off-axis at another angle θ_A as depicted in Fig. 1(c). As indicated previously, the coupled gain vanishes when phase-matched, rendering this useful mostly for frequency-conversion experiments from Stokes to anti-Stokes. A focusing beam contains a range of wavevectors, and choosing the correct F-number (with some light traveling at the angle θ_S) can partially satisfy the phase matching criterion while still allowing some coupled gain. However, when a collimated or weakly-focused laser generates the Stokes wave, the two waves will copropagate, and the phase mismatch cannot be avoided.

We can simplify the gain equation with four-wave mixing. By normalizing the coupled gain and the phase mismatch to the uncoupled gain α_R and approximating $h \approx 1$ (which is generally accurate for small Raman frequencies $\omega_v \ll \omega_L$), Eq. 3 becomes

$$\frac{g}{\alpha_R} = \sqrt{\frac{\Delta k}{\alpha_R}}\sqrt{-i - \frac{1}{4}\frac{\Delta k}{\alpha_R}}. \tag{4}$$

This normalization allows us to plot a single gain curve valid for any laser intensity as demonstrated in Fig. 1(d). We can clearly see that the FWM-related gain suppression only manifests for small phase mismatches $|\Delta k| \lesssim |\alpha_R|$. As the laser intensity and thus $|\alpha_R|$ increase, the wavenumber range affected by FWM also increases.

2.3. Kerr Self-Focusing

Next we consider a system subject to SRS, FWM, and Kerr self-focusing. The gain in Eq. 3 is calculated by setting $\alpha_1 = -(\alpha_R + \alpha_K)$, $\alpha_2 = -h(-\alpha_R + \alpha_K)$, $\kappa_1 = (\alpha_R + \alpha_K)$, and $\kappa_2 = h(-\alpha_R + \alpha_K)$, where $\alpha_K = 3i\omega_S\chi_{NR}|A_L|^2/(cn_S)$ is the positive imaginary Kerr phase contribution due to the strong laser field. The Kerr effect enhances the coupled gain when $\Delta k > 0$ but suppresses gain when $\Delta k < 0$ as shown in Fig. 2(a). Both gain suppression and gain enhancement have been demonstrated in silica fibers by tuning the laser about the zero-dispersion wavelength [8, 9]. Notably, at wavelengths with normal dispersion, Δk is always negative, so the Kerr effect will only suppress the coupled gain. We again consider the case of water at 355 nm ($\Delta k = -550$ cm^{-1}). As shown in Fig. 2(a), this wavelength always exhibits suppressed gain regardless of the laser intensity.

We can also simplify the gain equation when Kerr focusing is included. Again taking $h \approx 1$, Eq. 3 becomes

$$\frac{g}{\alpha_R} = \sqrt{\frac{\Delta k}{\alpha_R}}\sqrt{-i + |\chi_{NR}/\chi_{RS}| - \frac{1}{4}\frac{\Delta k}{\alpha_R}}. \tag{5}$$

In Fig. 2(b) we plot Eq. 5 for the ratio $|\chi_{NR}/\chi_{RS}| = 2.94$ characteristic of water at 355 nm. The enhanced gain occurs at a phase mismatch of $\Delta k/\alpha_R \approx 2|\chi_{NR}/\chi_{RS}|$ and reaches a gain of $\mathrm{Re}[g]/\alpha_R \approx \sqrt{1 + |\chi_{NR}/\chi_{RS}|^2}$. A similar enhancement factor has been demonstrated in silica fibers at laser wavelengths above the zero-dispersion wavelength [9, 10]. Importantly, the maximum Raman gain depends strongly on the nonresonant suceptibility χ_{NR}.

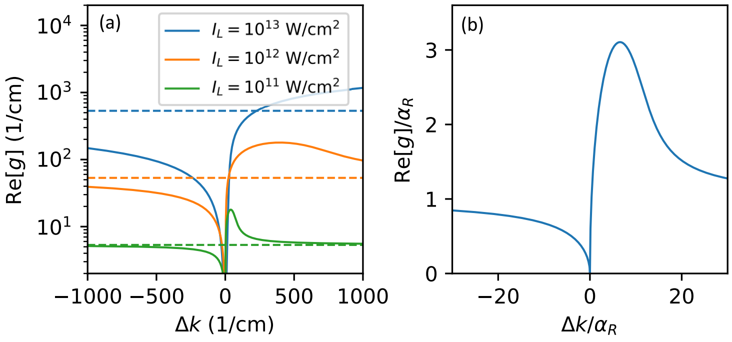

Fig. 2. Coupled gain spectrum including four-wave mixing and the Kerr nonlinearity. (a) Coupled gain (solid lines) and decoupled gain without FWM (dashed lines) in water for a 355 nm laser with three different intensities. (b) The approximate coupled gain spectrum normalized to the decoupled gain α_R is valid at any intensity.

Previous works demonstrating gain suppression and enhancement were limited to relatively low, ~100 W laser powers in silica fibers, reaching intensities of ~ 10^9 W/cm^2 [8, 9]. At these intensities, gain enhancement occurs only at a low, positive phase mismatch of order $\Delta k \sim m^{-1}$, corresponding to a wavelength range on the order of 10 nm wide in silica. Based on these results, we would not expect any gain enhancement for materials with normal dispersion where $\Delta k < 0$, e.g. in water at visible or UV wavelengths. We rather expect gain suppression over a larger wavelength range, since the condition $|\Delta k| \ll \alpha_R$ for gain suppression is more likely to be satisfied at high intensities. Figure 2(a) demonstrates this, showing the coupled gain in the region $\Delta k < 0$ to dip far below the uncoupled gain as the intensity increases. It is unclear how any such system could expect to experience enhanced gain.

2.4. Plasma Refraction

Plasma generation is a natural consequence of focusing megawatt-class lasers in condensed media, yet to our knowledge its effects on SRS in condensed media have not previously been explored. We now show that the presence of a low-density plasma can lead to strong gain enhancement almost without regard to the phase mismatch Δk. To capture the effects of the plasma refraction in Eqs. 2a and 2b, we set $\alpha_1 = -(\alpha_R + \alpha_K + \alpha_p)$ and $\alpha_2 = -h(-\alpha_R + \alpha_K + h_p\alpha_p)$ where $\alpha_p = -i\omega_p^2/(2c\omega_S n_S)$ is the negative, imaginary phase contribution due to the plasma, ω_p the plasma frequency, and $h_p = \omega_S^2/\omega_A^2$ a constant. We keep $\kappa_1 = (\alpha_R + \alpha_K)$ and $\kappa_2 = h(-\alpha_R + \alpha_K)$ as before.

Inserting these coefficients into Eq. 3 and approximating $h \approx h_p \approx 1$, we arrive at the normalized gain

$$\frac{g}{\alpha_R} = \sqrt{\frac{\Delta k + 2|\alpha_p|}{\alpha_R}}\sqrt{-i + |\chi_{NR}/\chi_{RS}| - \frac{1}{4}\left(\frac{\Delta k + 2|\alpha_p|}{\alpha_R}\right)}, \tag{6}$$

which reaches a maximum when

$$(\Delta k + 2|\alpha_p|)/\alpha_R \approx 2|\chi_{NR}/\chi_{RS}|. \tag{7}$$

We see in Eqs. 6 and 7 that the plasma effectively increases the phase mismatch Δk by a factor $|\alpha_p|$, thereby lowering the system's zero-dispersion wavelength. Fig. 3(a) illustrates this effect at laser intensity $I_L = 10^{12}$ W/cm^2, showing that higher plasma density allows Raman gain enhancement even for $\Delta k < 0$ where the medium has normal dispersion. In Fig. 3(b) we plot the gain for fixed $\Delta k = -550$ cm^{-1} and varied plasma density, clearly showing how increased plasma density permit gain enhancement.

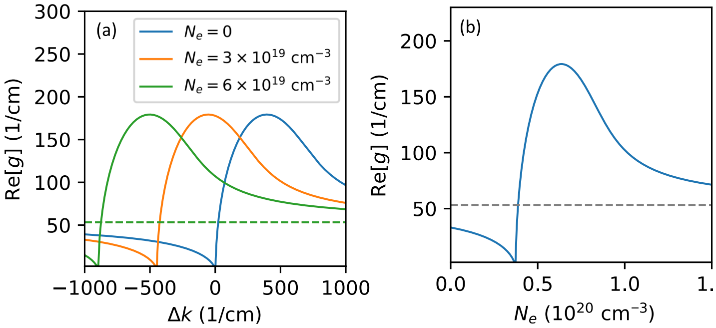

Fig. 3. Coupled gain spectrum including four-wave mixing, Kerr focusing, and plasma refraction. (a) Coupled gain (solid lines) and decoupled gain (dashed lines) in water for a 355 nm laser with intensity $I_L = 10^{12}$ W/cm^2 for three different plasma electron densities N_e. (b) Coupled gain at the copropagating phase mismatch $\Delta k = -550$ cm^{-1} for different plasma densities with laser intensity $I_L = 10^{12}$ W/cm^2.

2.5. *Intensity clamping*

The plasma density can be easily related to the intensity at focus. When the laser power P_L exceeds the Kerr critical power ($P_{cr} \approx 0.19\lambda_L^2 n_L \epsilon_0 c/\chi_{NL}$ with ϵ_0 the vacuum permittivity), or about 300 kW in water at 355 nm, self-focusing overpowers diffraction and the laser intensity will rise until ionization stops the self-focusing. This suggests that at focus, diffraction and plasma together must balance self-focusing; mathematically, we write this as

$$\alpha_p + \alpha_d \approx \alpha_K, \tag{8}$$

where $\alpha_d = \alpha_K(P_{cr}/P_L)$ is the phase change due to diffraction. Considering $P_L \gg P_{cr}$, we see that diffraction becomes unimportant for intensity clamping, and $\alpha_p \approx \alpha_K$. By setting $|\alpha_p| = |\alpha_K|$ in Eq. 7, the condition for maximum enhanced gain reduces to simply

$$\Delta k + 2|\alpha_K| \approx 2|\alpha_K|, \tag{9}$$

or alternatively

$$|\alpha_K| \gg |\Delta k|/2. \tag{10}$$

The condition in Eq. 10 can be easily converted to a laser intensity threshold by expanding α_K; we find that for any laser intensity at focus above approximately

$$I_T = \frac{c^2 n_S n_L \epsilon_0}{3\omega_S \chi_{NR}}|\Delta k|, \tag{11}$$

we expect nearly perfect phase matching and strongly enhanced SRS gain. This limit, which is $I_T \approx 2 \times 10^{12}$ W/cm^2 in water at 355 nm, considers copropagating laser and Stokes beams. With strong self-focusing, however, even a collimated or weakly-focused beam can lead to off-axis propagation angle θ_S of a few degrees. Fortunately, in water, even θ_S of a few degrees will only affect Δk and I_T by a factor of order unity; as long as the $I_L \gg I_T$ for a collimated beam, it is likely to hold with self-focusing as well. Our last step is to understand when this threshold will be reached.

3. Full spatiotemporal dynamics

Predicting the peak intensity at focus is difficult, as it depends on multiple nonlinear and spatiotemporally-dependent processes including pump depletion and ionization. This leads us to numerical methods. Full three-wave nonlinear envelope propagation equations have been derived previously including both Raman and Kerr susceptibilities [19], four-wave mixing, and ionization [20] with 2D axisymmetry in pulse-frame longitudinal, temporal and radial coordinates z, $\tau = t - z/v_{gL}$, and r.

We model the plasma dynamics including both multiphoton and collisional ionization. The electron density N_e evolves according to

$$\frac{\partial N_e}{\partial \tau} = \nu_{\text{MPI}} N_0 - \eta N_e, + \nu_i N_e \tag{12}$$

where N_0 is the density of neutrals, η the electron reattachment rate, ν_{MPI} the total multiphoton ionization rate, and ν_i the collisional ionization rate. In water, we set $N_0 = 3.34 \times 10^{22}$ cm^{-3} and $\eta = 10^{12}$ s^{-1}. Recombination is negligible compared to electron reattachment, as $\beta_r N_e \ll \eta$ for the electron densities in our study and recombination coefficient $\beta_r \sim 2 \times 10^{-9}$ cm^3/s [21]. The multiphoton ionization rate is given by

$$\nu_{\text{MPI}} = \sum_{n=S,L,A} \nu_{\text{MPI},n}, \tag{13a}$$

$$\nu_{\text{MPI},n} = \frac{2\pi}{(l-1)!}\omega_n \left[\frac{I_n}{I_{\text{MPI}}}\right]^l, \tag{13b}$$

where l is the number of photons to ionize an electron with photons exclusively of frequency ω_n, and I_{MPI} is the characteristic multiphoton ionization rate constant. For our test case in water, we extract I_{MPI} from the field ionization model introduced by Keldysh64 for crystalline media, due to the polycrystalline nature of water with conduction band energy $U_{\text{ion}} \approx 9.5$ eV [3,22]. We find that for an electron effective mass $m_{\text{eff}} = 0.2\, m_e$ [3] (where m_e is the free electron mass), laser wavelength 355 nm, and intensity $I_L \lesssim 10^{13}$ W/cm^2, the full Keldysh model predicts simple multiphoton ionization with a characteristic intensity of $I_{\text{MPI}} = 1.6 \times 10^{15}$ W/cm^2.

The collisional ionization rate ν_i and electron collision frequency ν_e obey

$$\nu_i = \frac{\nu_e}{U_{\text{ion}}}\frac{2e^2}{m_{\text{eff}}} \sum_{n=S,L,A} \frac{|A_n|^2}{\omega_n^2}, \tag{14a}$$

$$\nu_e = N_0 \sigma_c \frac{e\sqrt{2}}{m_{\text{eff}}} \left(\sum_{n=S,L,A} \frac{|A_n|^2}{\omega_n^2} \right)^{1/2}, \tag{14b}$$

where $-e$ is the electron charge, and σ_c the collisional ionization cross section which we set to 3.1×10^{16} cm^{-2} in accordance with electron impact ionization and scattering time experiments in water [23,24].

Finally, the paraxial, slowly-varying envelope propagation equations are written [15]

$$\begin{aligned} 2ik_S \frac{\partial A_S}{\partial z} &+ \frac{\partial^2 A_S}{\partial r^2} + \frac{1}{r}\frac{\partial A_S}{\partial r} - k_S \beta_S'' \frac{\partial^2 A_S}{\partial \tau^2} + 2ik_S \left(\frac{1}{v_{gS}} - \frac{1}{v_{gL}}\right)\frac{\partial A_S}{\partial \tau} - \frac{\omega_p^2}{c^2}\left(1 - \frac{i\nu_e}{\omega_S}\right) A_S \\ &+ \frac{i\omega_S}{2c^2}\frac{U_{\text{ion}}}{|A_S|^2} N_0 \nu_{\text{MPI},S} A_S = \frac{-6\omega_S^2}{c^2}\left[\frac{1}{2}\chi_{NR}|A_S|^2 A_S + (\chi_{RS} + \chi_{NR})|A_L|^2 A_S \right. \\ &\left. + \chi_{NR}|A_A|^2 A_S + (\chi_{RS} + \chi_{NR}) A_L^2 A_A^* e^{i\Delta k z}\right], \end{aligned} \tag{15a}$$

$$\begin{aligned}
&2ik_L\frac{\partial A_L}{\partial z}+\frac{\partial^2 A_L}{\partial r^2}+\frac{1}{r}\frac{\partial A_L}{\partial r}-k_L\beta_L''\frac{\partial^2 A_L}{\partial \tau^2}-\frac{\omega_p^2}{c^2}\left(1-\frac{i\nu_e}{\omega_L}\right)A_L\\
&\quad+\frac{i\omega_L}{2c^2}\frac{U_{\text{ion}}}{|A_L|^2}N_0\nu_{\text{MPI},L}A_L=\frac{-6\omega_L^2}{c^2}\Bigg[(\chi_{RA}+\chi_{NR})|A_S|^2A_L+\frac{1}{2}\chi_{NR}|A_L|^2A_L\\
&\quad+(\chi_{RS}+\chi_{NR})|A_A|^2A_L+2\chi_{NR}A_L^*A_SA_Ae^{-i\Delta kz}\Bigg],
\end{aligned}\tag{15b}$$

$$\begin{aligned}
&2ik_A\frac{\partial A_A}{\partial z}+\frac{\partial^2 A_A}{\partial r^2}+\frac{1}{r}\frac{\partial A_A}{\partial r}-k_A\beta_A''\frac{\partial^2 A_A}{\partial \tau^2}+2ik_A\left(\frac{1}{v_{gA}}-\frac{1}{v_{gL}}\right)\frac{\partial A_A}{\partial \tau}-\frac{\omega_p^2}{c^2}\left(1-\frac{i\nu_e}{\omega_A}\right)A_A\\
&\quad+\frac{i\omega_A}{2c^2}\frac{U_{\text{ion}}}{|A_A|^2}N_0\nu_{\text{MPI},A}A_A=\frac{-6\omega_A^2}{c^2}\Bigg[\chi_{NR}|A_S|^2A_A+(\chi_{RA}+\chi_{NR})|A_L|^2A_A\\
&\quad+\frac{1}{2}\chi_{NR}|A_A|^2A_A+(\chi_{RA}+\chi_{NR})A_L^2A_S^*e^{i\Delta kz}\Bigg].
\end{aligned}\tag{15c}$$

with $\omega_p=\sqrt{N_e e^2/m_{\text{eff}}\epsilon_0}$ the plasma frequency, $v_{gn}=1/\beta_n'$ the group velocity at frequency ω_n, $\beta_n'=\partial\beta(\omega)/\partial\omega|_{\omega=\omega_n}$, and $\beta_n''=\partial^2\beta(\omega)/\partial\omega^2|_{\omega=\omega_n}$.

4. Numerical simulation

We solve the system in Eqs. 12,15a,15b, and 15c numerically with the SNOPROP simulation code [15,16]. The system is initialized with a temporally and radially gaussian laser pulse, while the Stokes and anti-Stokes fields are initialized to a uniform background intensity $I_{\text{BG}}=10^{-2}$ W/cm^2 [1,25]. Our first example consists of a 4 MW, 355 nm, 0.5 ps laser pulse with 192 μm FWHM focusing in water with F-number of 42 (geometric focus at $z=0.8$ cm). All additional simulation parameters are reported in Table 1. We perform two simulations: the first solves the equations as written, while the second disables four-wave mixing by setting $e^{i\Delta kz}\to 0$ and $e^{-i\Delta kz}\to 0$ in Eqs. 15a,15b, and 15c.

Table 1. Simulation parameters for 0.5 ps pulse

Radial box size		800 μm
Radial cell size	dr	0.25 μm
Temporal box size		3 ps
Temporal cell size	$d\tau$	25 fs
Simulation length		1.6 cm
Step size	dz	2 μm
Stokes refractive index	n_S	1.3493
Laser refractive index	n_L	1.3572
Anti-Stokes refractive index	n_A	1.3662
Stokes group index	n_{gS}	1.4040
Laser group index	n_{gL}	1.4269
Anti-Stokes group index	n_{gA}	1.4558

The energy exchange between the three waves is shown in Fig. 4 with and without four-wave mixing enabled. In panel (a) we see that the the Stokes power output increases from 12% to 39% of the input power when four-wave mixing is enabled, and the output laser power decreases from 60% to 35% of the input power. Anti-Stokes light is understandably only produced when four-wave mixing is enabled. The log-scale power evolution in panel (b) illustrates the Stokes gain enhancement, raising the peak Stokes growth rate from 160 cm^{-1} to 540 cm^{-1}. This gain enhancement factor of 3.38 is close to the expected enhancement factor $\sqrt{1+|\chi_{NR}/\chi_{RS}|^2} \sim 3.16$ due to four-wave mixing with the plasma-assisted phase matching. Panel (c) confirms that the peak laser intensity remains well above the threshold $I_T = 1.8 \times 10^{12}$ W/cm^2 for enhanced SRS as the laser propagates through focus, and even the average laser intensity (here calculated as the maximum intensity after averaging over the temporal FWHM) is comparable to the threshold.

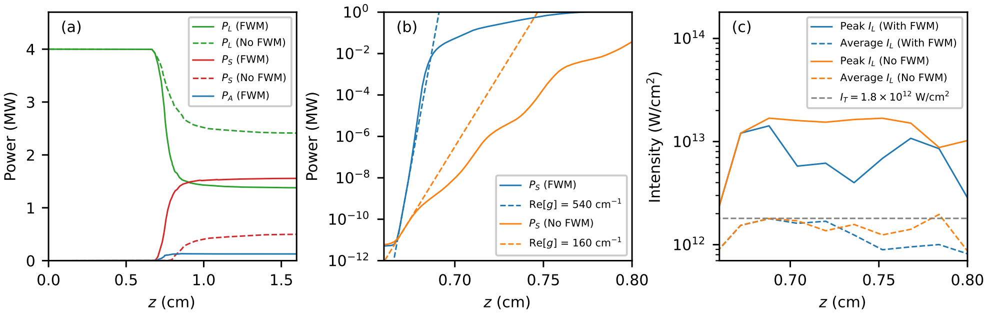

Fig. 4. Evolution of a 0.5 ps laser pulse propagating through focus in water. (a) Power of each of the three waves in simulations with and without FWM enabled. (b) Stokes power growth with approximate exponential fits. (c) Peak laser intensity and highest temporally-averaged laser intensity with FWM compared to the threshold for gain enhancement.

Oscillations in the Stokes gain (c.f. Fig. 4(b)) correspond to spatiotemporal modulation of the laser profile (c.f. Fig. 5(b)) by an ionization instability [26]. The instability transversely corrugates both the laser envelope and the electron density with a spatial scale near the plasma wavelength; the peak electron density of $N_e \sim 10^{20}$ cm^{-3} corresponds to a plasma wavelength $\lambda_p = 2\pi c/\omega_p \sim 3$ μm, which is similar to the scale in Fig. 5(b). Since the center of the pulse ($\tau = 0$) has the highest power (well above P_{crit}), it will self-focus first, followed later by slices near the head of the pulse. This causes the instability-generated corrugations to travel along the pulse in the $-\tau$ direction. We see in Fig. 5 that over a distance ~64 μm, two intensity nodes cross the center of the pulse at $\tau = 0$, simultaneous with two gain oscillations in Fig. 4(b)). This confirms that the gain modulations are related to the ionization instability and underscores the importance of a full spatiotemporal treatment of the separate waves to accurately predict SRS.

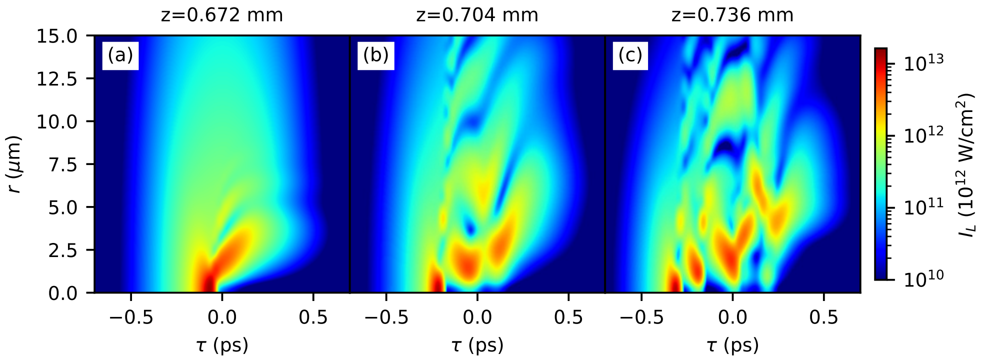

Fig. 5. Intensity profiles of a 0.5 ps laser pulse focusing in water with FWM disabled. (a,b,c) The laser envelope is shown at three different positions in z, with the front of the laser pulse at negative τ.

In order to understand the effect of the gain enhancement at lower intensities, we simulate an additional system where a 5 ps laser pulse focuses with a larger F-number of 80 and longer propagation distance of 3.2 cm. The temporal box and cell size are increased by a factor of 10, but all other parameters are as in Table 1. The longer pulse duration will enhance collisional ionization and reduce the laser intensity at focus. The energy evolution in Fig. 6(a) differs dramatically from the case with the shorter pulse, as enabling FWM only increases the output Stokes power by 2% and decreases the laser output power by 5%. However, Fig. 6(b) shows a clear enhancement in the exponential Stokes gain rate by a factor of 3.28—once again close to the expected theoretical enhancement of 3.16. Fig. 6(b) resolves the contradiction; we see that while the peak laser intensity exceeds I_T, allowing very localized regions near the high-intensity lobes (c.f. Fig. 5) to experience enhanced gain, the temporally-averaged laser intensity remains well below I_T and the majority of the laser energy does not experience enhanced gain. We confirm that the FWM-enhanced SRS gain is only to be expected at sufficiently high intensities above I_T.

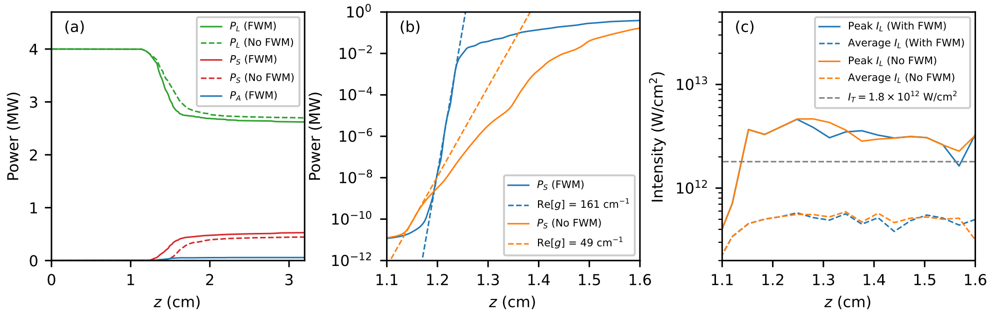

Fig. 6. Evolution of a 5 ps laser pulse propagating through focus in water. (a) Power of each of the three waves in simulations with and without FWM enabled. (b) Stokes power growth with approximate exponential fits. (c) Peak laser intensity and highest temporally-averaged laser intensity with FWM compared to the threshold for gain enhancement.

5. Conclusion

We have shown that four-wave mixing can significantly enhance Raman gain when high-power lasers focus in condensed media. Our analytical results agree well with multidimensional nonlinear laser propagation simulations and confirm that above a certain threshold intensity I_T, the laser-generated plasma provides the ideal phase matching for enhanced gain over a broad wavelength range. This enhanced gain can lead to many times higher Stokes Raman production and vastly increased laser energy losses. Accurate prediction of the Raman gain at high intensities may require a fully-spatiotemporal treatment of each of the Stokes, laser, and anti-Stokes waves. Water-based experiments similar to Ref. [3] but with shorter laser pulses could experimentally verify this gain enhancement. Although we primarily consider laser propagation in water, the phenomenon may also occur in other dielectrics which are weakly ionized by a high-intensity, several-critical-power laser.

6. Funding

J. R. P. acknowledges support by the National Science Foundation under award number PHY – 1903414, as well as the DOE NNSA LRGF fellowship under cooperative agreement number DE-NA0003960.

7. Acknowledgements

We thank S. Glenzer for helpful discussions.

References

1. M. Sceats, S. A. Rice, and J. E. Butler, "The stimulated raman spectrum of water and its relationship to liquid structure," The J. Chem. Phys. **63**, 5390–5400 (1975).
2. B. Hafizi, J. P. Palastro, J. R. Peñano, T. G. Jones, L. A. Johnson, M. H. Helle, D. Kaganovich, Y. H. Chen, and A. B. Stamm, "Stimulated raman and brillouin scattering, nonlinear focusing, thermal blooming, and optical breakdown of a laser beam propagating in water," J. Opt. Soc. Am. B **33**, 2062–2072 (2016).
3. Y.-H. Chen, J. R. Peterson, L. A. Johnson, T. G. Jones, B. Hafizi, A. B. Stamm, A. C. Ting, J. P. Palastro, M. H. Helle, and D. Kaganovich, "Ionization in the field of a strong electromagnetic wave," Opt. Lett. **45**, 4344–4347 (2020).
4. Y. Ganot, S. Shrenkel, B. D. Barmashenko, and I. Bar, "Enhanced stimulated raman scattering in temperature controlled liquid water," Appl. Phys. Lett. **105**, 061107 (2014).
5. M. H. Helle, T. G. Jones, J. R. Peñano, D. Kaganovich, and A. Ting, "Formation and propagation of meter-scale laser filaments in water," Appl. Phys. Lett. **103**, 121101 (2013).
6. N. Bloembergen and Y. R. Shen, "Coupling between vibrations and light waves in raman laser media," Phys. Rev. Lett. **12**, 504–507 (1964).
7. S. Trillo and S. Wabnitz, "Parametric and raman amplification in birefringent fibers," J. Opt. Soc. Am. B **9**, 1061–1082 (1990).
8. E. Golovchenko, P. V. Mamyshev, A. N. Pilipetskii, and E. M. Dianov, "Mutual influence of the parametric effects and stimulated raman scattering in optical fibers," IEEE J. Quantum Electron. **26**, 1815–1820 (1990).
9. F. Vanholsbeeck, P. Emplit, and S. Coen, "Complete experimental characterization of the influence of parametric four-wave mixing on stimulated raman gain," Opt. Lett. **28**, 1960–1962 (2003).
10. A. S. Y. Hsieh, G. K. L. Wong, S. G. Murdoch, S. Coen, F. Vanholsbeeck, R. Leonhardt, and J. D. Harvey., "Strong signal suppression in single-pump optical parametric amplifiers," Opt. Express **15**, 8104–8114 (2007).
11. W. Liu, P. Ma, P. Zhou, and Z. Jiang, "Effects of four-wave-mixing in high-power raman fiber amplifiers," Opt. Express **28**, 593–606 (2020).
12. A. Vogel, J. Noack, G. Hüttman, and G. Paltauf, "Mechanisms of femtosecond laser nanosurgery of cells and tissues," Appl. Phys. B **81**, 1015–1047 (2005).
13. T. G. Jones, A. Ting, D. Gordon, M. Helle, and J. Peñano, "Underwater laser-guided discharge," U.S. Pat. 8,941,967 (2015).
14. T. G. Jones, A. Ting, D. F. Gordon, M. H. Helle, and J. R. Peñano, "Two-laser generation of extended underwater plasma," U.S. Pat. 9,088,123 (2015).
15. J. R. Peterson, T. G. Jones, B. Hafizi, L. A. Johnson, and D. F. Gordon, "SNOPROP: a solver for nonlinear optical propagation," (2020). Memorandum Report, NRL/MR/6795–20-10,121 (Naval Research Laboratory).
16. J. R. Peterson, "SNOPROP: a solver for nonlinear optical propagation," Zenodo (2020).
17. R. W. Boyd, *Nonlinear Optics* (Academic Press, Burlington, 2008), 3rd ed.

18. D. A. Akimov, E. E. Serebryannikov, A. M. Zheltikov, M. Schmitt, R. Maksimenka, W. Kiefer, K. V. Dukel'skii, V. S. Shevandin, and Y. N. Kondrat'ev, "Efficient anti-stokes generation through phase-matched four-wave mixing in higher-order modes of a microstructure fiber," Opt. Lett. **28**, 1948–1950 (2003).
19. N. Bloembergen, *Nonlinear Optics* (Harvard University, 1996), 4th ed.
20. P. Sprangle, J. R. Peñano, and B. Hafizi, "Propagation of intense short laser pulses in the atmosphere," Phys. Rev. E **66**, 046418 (2002).
21. F. Docchio, "Lifetimes of plasmas induced in liquids and ocular media by single nd:yag laser pulses of different duration," Eur. Lett. **6**, 5 (1988).
22. F. Williams, S. P. Varma, and S. Hillenius, "Liquid water as a lone-pair amorphous semiconductor," The J. Chem. Phys. **64**, 1549–1554 (1976).
23. M. V. V. S. Rao, I. Iga, and S. K. Srivastava, "Ionization cross-sections for the production of positive ions from H_2O by electron impact," J. Geophys. Res. **100**, 26421–26425 (1995).
24. C. Sarpe, J. Köhler, T. Winkler, M. Wollenhaupt, and T. Baumert, "Real-time observation of transient electron density in water irradiated with tailored femtosecond laser pulses," New J. Phys. **14**, 075021 (2012).
25. M. Colles, "Efficient stimulated raman scattering from picosecond pulses," Opt. Commun. **1**, 169 – 172 (1969).
26. J. Thomas M. Antonsen and Z. Bian, "Ionization induced scattering of short intense laser pulses," Phys. Rev. Lett. **82**, 3617–3620 (1999).